π-Conjugated Electroactive Oligomers: Energy and Electron Transducing Systems

Dirk M. Guldi,* Chuping Luo, and Angela Swartz

Radiation Laboratory, University of Notre Dame, Notre Dame, Indiana 46556

Rafael Gómez, José L. Segura, and Nazario Martín*

Departamento de Química Orgánica, Facultad de Química, Universidad Complutense, E-28040 Madrid, Spain

Received: January 23, 2003; In Final Form: October 6, 2003

Suitably difunctionalized oligomers have been used to synthesize a series of novel, soluble, and strongly fluorescent C_{60}-conjugated oligomer triads through 1,3-dipolar cycloaddition reactions. The nature of the oligomeric components have been modified to tailor (i) the absorption wavelength of the chromophore and (ii) the oxidation potential of the oligomeric donor moiety. The resulting triads were examined by electrochemical and photophysical techniques. Both singlet−singlet energy transfer and intramolecular electron transfer were found to take place and to compete with each other in the overall deactivation of the photoexcited chromophores. Strong electronic couplings between the donor and acceptor moieties not only affect the ground-state spectra, which exhibit marked red shifts, but, more importantly, give rise to ultrafast electron and energy transfer reactions. In terms of stabilizing the product and enhancing the yield of charge separation, comparison with previously reported analogues containing only a single fullerene unit (i.e., dyad) shows that particular benefits were noted by attaching two fullerene cores (i.e., triad) to the oligomeric structure.

Introduction

During the past decade conjugated polymers have been extensively probed as new and promising materials for photovoltaic applications.[1] Hereby, intense efforts were directed towards the development of solid-state polymer photovoltaic cells, based on composite films, that are blends of conjugated polymers and functionalized fullerene derivatives.[2,3] Utilizing electron-accepting fullerenes in combination with π-conjugated systems, as sacrificial electron donors, offers several attractive features. In particular, fullerenes, due to their low reorganization energy in electron-transfer reactions, accelerate charge separation and decelerate charge recombination, compared to two-dimensional, planar electron acceptors. This, as a whole, is beneficial for stabilizing the charge-separated state in C_{60}-based materials—the ultimate motivation in artificial electron transfer systems. In this regard, it also appeared attractive to us that well-structured oligomers facilitate, similarly to their related polymers, charge delocalization within their structures.

Thus, several dyad[4,5] structures, consisting of different conjugated oligomers covalently linked to one fullerene core, have been probed as bicontinuous networks in time-resolved and steady-state photolytic experiments. These donor−acceptor arrays give rise to fundamentally different photophysical behavior (i.e., energy versus electron transfer), whose outcome depends largely on the nature of the π-conjugated oligomeric system as well as on the number of repeating units in the oligomer.

Far less investigated are the related triads,[6] consisting of conjugated oligomers covalently linked to two fullerene cores, see Chart 1. It is worth mentioning that, to the best of our knowledge, so far only heterocyclic containing oligomers, such as thiophene (**1**, **3**) and pyrrol (**2**, **4**) have been used as π-conjugated spacers.

In the present contribution, we describe a series of new oligomeric model systems covalently linked to two fullerene moieties (**5a**−**d**, Chart 2). In particular, different arylene units ranging from naphthalene and benzene to thiophene with diverse electrochemical and excited-state properties have been incorporated into π-conjugated backbones.

Fine-tuning the electrochemical and photophysical properties of the π-conjugated systems allows us not only to impact the overall thermodynamics (i.e., facilitate or retard intramolecular electron-transfer processes) but also to influence the competition between the dominant singlet−singlet energy transfer and electron transfer events (i.e., shifting the deactivation of the photoexcited chromophore from an energy to an electron transfer scenario).

Results and Discussion

Synthesis. Among the suitable procedures for the functionalization of C_{60}, the 1,3-dipolar cycloaddition of azomethine ylides plays a dominant role.[7] To date, a large number of fulleropyrrolidine derivatives, bearing different electro- or photoactive addends or both, have been synthesized following the basic concept of this procedure.[8] This led us to select this synthetic approach for the preparation of target triads **5a**−**d**, which were obtained by reacting sarcosine, C_{60}, and the corresponding π-conjugated system functionalized with two aldehyde groups (**6a**−**d**,[9] Scheme 1) in refluxing toluene for 24 h.

Due to the presence of the long alkoxy substituents, **5b**−**d** are soluble in common organic solvents, and complete spectroscopic characterization was subsequently achieved. Compound **5a** showed only limited solubility that, however, allowed its spectroscopic characterization. It is worth mentioning that

* To whom correspondence should be addressed. E-mail address for N.M.: nazmar@quim.ucm.es.

10.1021/jp034186a CCC: $27.50
Published on Web 12/18/2003

CHART 1

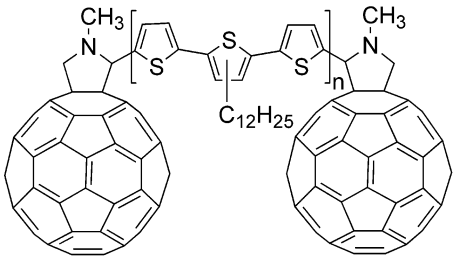

1: n= 1-3

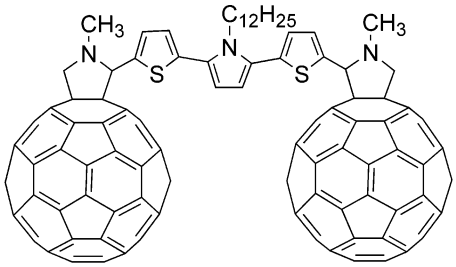

2

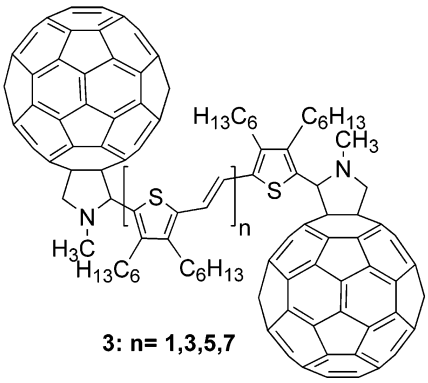

3: n= 1,3,5,7

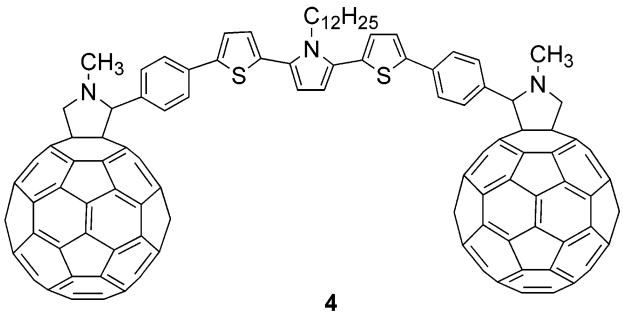

4

CHART 2

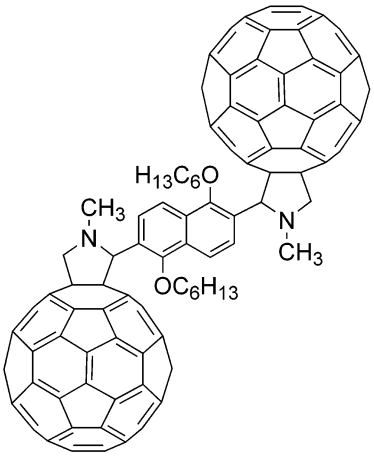

5a

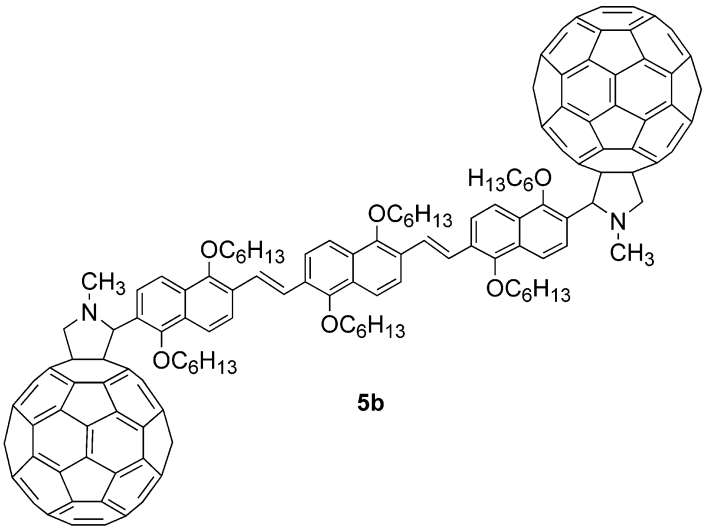

5b

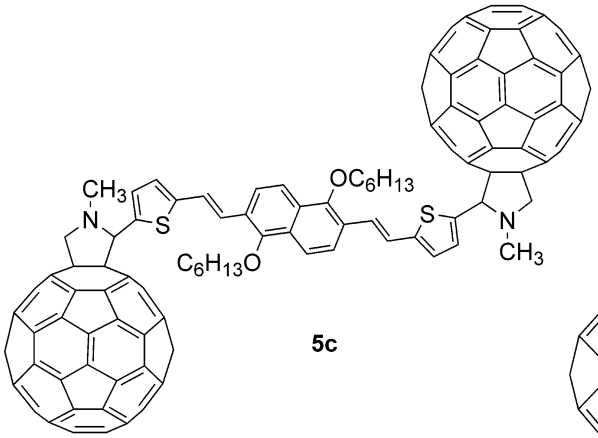

5c

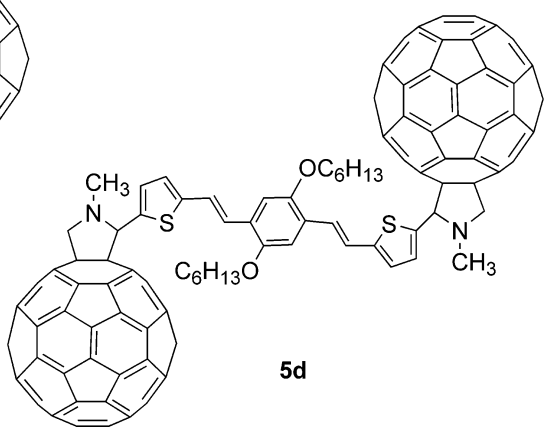

5d

the cycloaddition reaction creates new stereocenters at each pyrrolidine ring, and therefore, **5a**−**d** are obtained as a mixture of diastereoisomers which, however, only in some cases could be separated chromatographically.

SCHEME 1

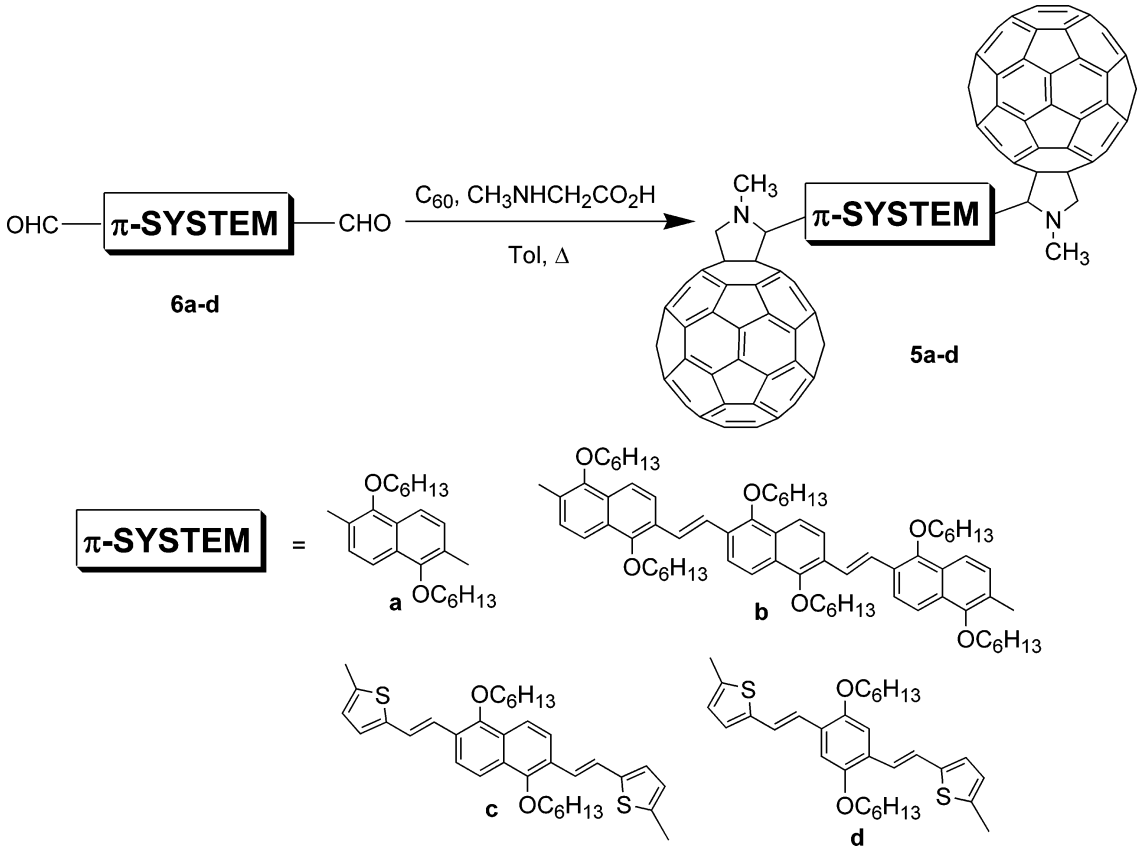

The ^{1}H NMR spectra of the compounds in $CDCl_3$ solution confirm that the stereochemistry *E* ($J \approx 16$ Hz) of the vinylenic double bonds remains unaffected after the cycloaddition reaction. As far as C_{60} is concerned, its diagnostic signals appear at around 5.1 ppm (CH) as a singlet and a set of two doublets (CH_2) with coupling constants around $J = 9.8$ Hz. The low solubility exhibited by these triads prevented us from recording the ^{13}C NMR spectra in common deuterated solvents. Nevertheless, the structures of the synthesized triads were ascertained by means of the elemental analyses, as well as the mass spectroscopy by using APCI (Atmospheric Pressure Chemical Ionization) and ESI (Electro Spray Ionization) techniques.

Electrochemistry. The electrochemical features of **5a**−**d** were investigated by cyclic voltammetry (CV) at room temperature. Dichloromethane as solvent and tetra-*n*-butylammonium perchlorate as supporting electrolyte were used in a conventional three-compartment cell, equipped with glassy carbon, SCE, and platinum wire as working electrode, reference electrode, and auxiliary electrode, respectively. The redox potentials are collected in Table 1 and compared with those of unsubstituted π-conjugated **7a**−**d**[4b] and fulleropyrrolidine **8** as reference compounds (Chart 3).[10] The lack of solubility of **5a** prevented its electrochemical characterization.

In the cathodic scan region, C_{60}−oligomer−C_{60} triads (**5b**−**d**) show three quasireversible one-electron reduction waves that reflect the first three one-electron reduction steps of C_{60}. As a consequence of saturating a double bond of the C_{60} core, the reduction potential values of the triads are shifted to more negative values relative to that of pristine C_{60}.[11] As expected, the first reduction potential values found for **5b**−**d** were all similar.

The redox behavior of the conjugated π-systems (**7a**−**d**) shows an increase of the donor strength when going from dihexyloxynaphthalene (**7a**, $E_{ox} = 1.41$ V) to the trimeric analogue (**7b**, $E_{ox} = 1.31$ V) and also upon replacing the peripheral naphthalene units in the trimer by the π-excedent thiophene ring (**7c**, $E_{ox} = 1.20$ V). The best results, in terms of ease of oxidation, were observed for the π-conjugated system in which the central naphthalene moiety is replaced by a phenylene unit (**7d**, $E_{ox} = 1.01$ V). This trend is in good agreement with related studies on conjugated oligomers containing naphthalene, thiophene, and phenylene units.[12] Interestingly, **5b**, which bears the oligonaphthalenevinylene moiety, showed the oligomer oxidation wave at 1.44 V. Since this value is anodically shifted in comparison with the parent oligomer (**7b**, 1.31 V), it is indicative of some electronic interaction between the electron-accepting C_{60} and oligomer moiety in the ground state.[13]

TABLE 1: Redox Potentials (V, ±0.05 V) of Fullerene-Based Triads (5a−d) and Reference Compounds (7a−d and 8)

compd	E^1_{pa} [a]	E^1_{pc} [b]	E^2_{pc}	E^3_{pc}	E^4_{pc}
7a	1.41				
5a	*c*	*c*	*c*	*c*	*c*
7b	1.31				
5b	1.44	−0.65	−1.05	−1.62	−1.93
7c	1.20				
5c	*c*	−0.66	−1.02	−1.61	
7d	1.01				
5d	*c*	−0.64	−1.04	−1.65	
8	1.32	−0.71	−1.14	−1.75	

[a] pa = anodic peak. [b] pc = cathodic peak. In dichloromethane solution using Bu_4NClO_4 (0.3 mg L^{-1}, SCE reference electrode and glassy carbon as working electrode). [c] Not observed.

Photophysical Properties. *Oligomer References.* The features of the reference oligomers **7a**−**d** shall be gathered, as they were established in a number of steady-state and time-resolved

CHART 3

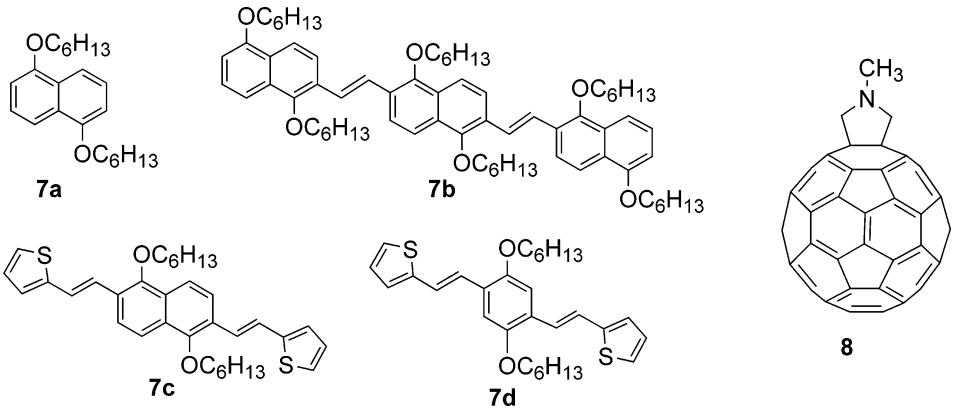

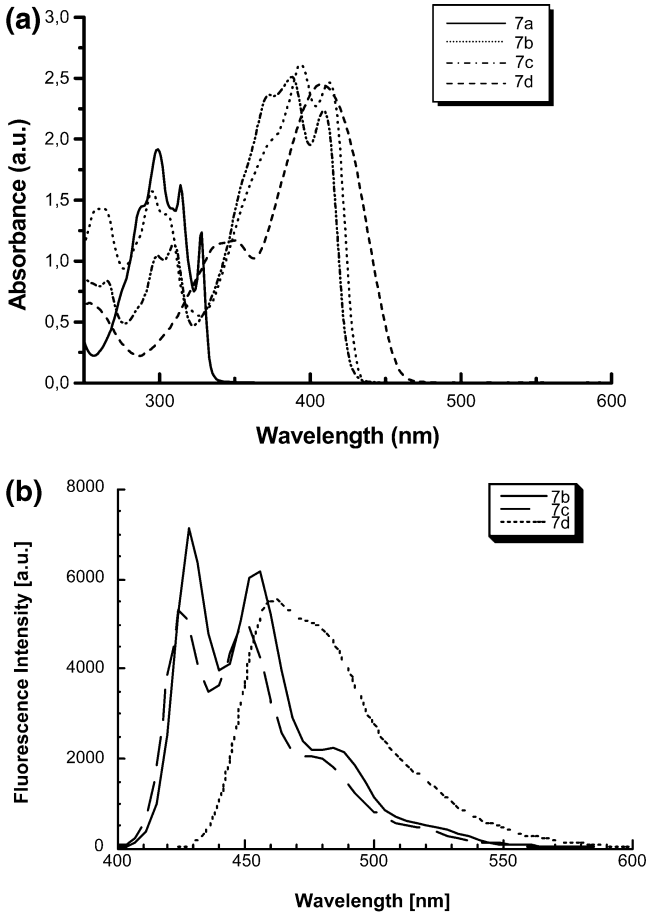

Figure 1. Absorption spectra (a) of references **7a**−**d** in dichloromethane and emission spectra (b) of references **7b**−**d** in toluene with matching absorption at the 410 nm excitation wavelength (i.e., $OD_{410\ nm} = 0.5$).

experiments, to serve as important references for the investigated triads (UV−vis absorption spectra of **7a**−**d** are shown in Figure 1a).

When the ground-state absorption of the 1,5-dihexyloxynaphthalene monomer is compared with its trimeric analogue, a strong red shift of the maximum is noted ($\lambda_{max} = 328$ nm → $\lambda_{max} = 413$ nm). This shift is in agreement with effects that stem from a more delocalized and extended π-system present in the trimeric structure. Although replacement of the two peripheral naphthalene units by two thiophene units and additional substitution of the central dihexyloxynaphthalene unit by 1,4-dihexyloxybenzene led to marked changes in the redox properties, the absorption maxima (**7c**, $\lambda_{max} = 412$ nm; **7d**, $\lambda_{max} = 412$ nm) nearly coincide with that of **7b**. Table 2 reviews all the ground- and excited-state properties of the investigated reference compounds.

All references are extremely strong fluorophores with quantum yields that approach unity, which renders them convenient probes for the photophysical measurements. Fluorescence spectra of the major references are shown in Figure 1b. The fluorescence spectra of the oligomer references are in excellent agreement with their mirror imaged absorption features. Most importantly, the sharp maxima of the *0−0 emission ($\lambda_{max} \approx$ 430 nm) differ only slightly from the 0−*0 absorption ($\lambda_{max} \approx$ 412 nm), which is indicative of small Stokes shifts. This assignment appears quite plausible, considering the rigid nature of the π-systems as an important parameter in determining the nuclear coordinates of the excited states relative to those of the ground state. The only exception to this eminent trend is **7d**. Parallel to the high fluorescence yields, the investigated models show relatively long-lived fluorescence.

To characterize the transient intermediates evolving from photoexcitation of the oligomer references, we probed **7a**−**d** by transient absorption spectroscopy following either 18 ps or 8 ns laser pulses. This approach allows spectral characterization of the photoexcited oligomers and kinetic analysis of their excited-state deactivation. All oligomer references (**7a**−**d**) display in their singlet excited states, besides their strong emissive features in the 400−550 nm range, characteristic singlet−singlet transitions. Following 20 ps laser pulse photoexcitation of **7b**, as an example, led to the instantaneous formation of a strong maximum in the 800−900 nm region. The transients are typically short-lived and exhibit monoexponential decay rates on the order of 10^9 s^{-1}. In the near-infrared, the absorption changes are governed by the disappearance of the singlet−singlet absorption, while in the blue region the simultaneous formation of new maxima was noted, see Figure 2.

Particularly important is that the time constant of the near-infrared decay is nearly identical with that of the visible growth. It is worthwhile to underline that these intersystem crossing (ISC) kinetics reveal an almost exact resemblance with the fluorescence lifetime. An additional test in support of the ISC hypothesis required examining the triplet absorption characteristics in nanosecond experiments, as an example, following 8 ns pulses, see Figure 3. In fact, the triplet−triplet maxima were in perfect accord with the spectral features observed at the end of the picosecond time scale.

In the presence of molecular oxygen, the triplet excited states of all reference oligomers (**7a**−**d**) experience a concentration-dependent deactivation process. Different oxygen concentrations,

TABLE 2: Photophysical Data of References[a]

compd	λ_{max}, ground state [nm]	energy, singlet excited state [eV]	Φ_{fluor} (toluene)	τ_{fluor} (toluene) [ns]	λ_{max}, singlet excited state [nm]	λ_{max}, triplet excited state [nm]	ISC (toluene) [s^{-1}]	$\tau_{triplet}$ (toluene) [μs]	k_{oxygen} (toluene) [M^{-1} s^{-1}]	λ_{max}, radical cation [nm]
8	690	1.76 (704 nm)	0.0006	1.38	900	700	5.5×10^8	20	1.6×10^9	1000
7b	413	2.89 (427 nm)	0.72	0.91	870	630	8.6×10^8	2.13	2.5×10^9	640
7c	412	2.91 (425 nm)	0.54	1.31	840	580	6.0×10^8	1.02	3.1×10^9	680
7d	412	2.70 (458 nm)	0.56	1.9	760	545	4.5×10^8	14.3	2.9×10^9	660

[a] For details on the data determination, see Experimental Section.

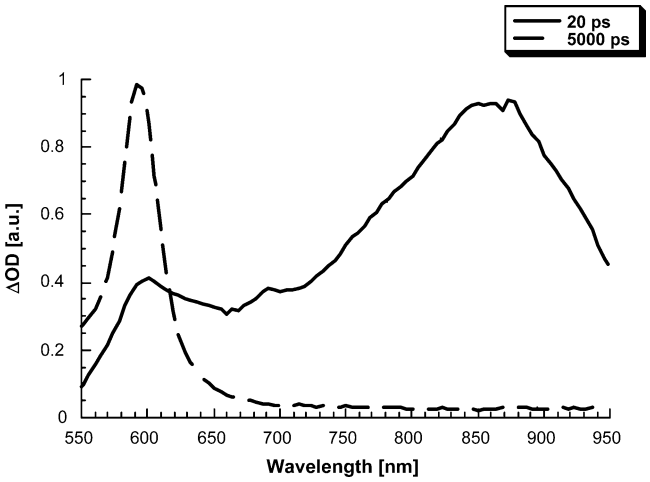

Figure 2. Transient absorption spectrum, visible−near-infrared part, recorded 20 ps (—) and 5000 ps (−••) after flash photolysis of reference **7b** (2.0×10^{-5} M) at 355 nm in deoxygenated toluene indicating the oligomer singlet−singlet and triplet−triplet features, respectively.

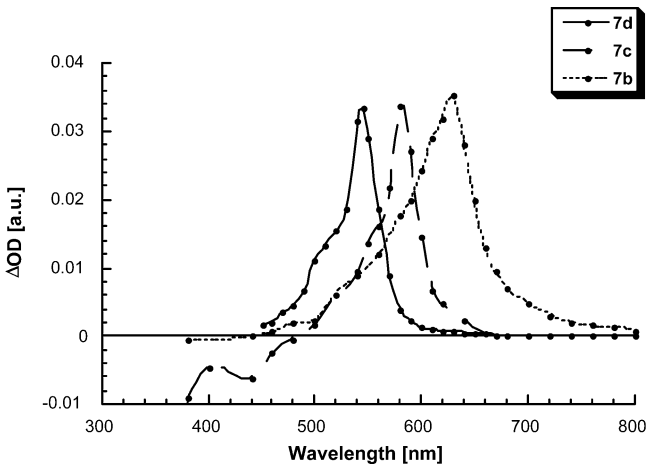

Figure 3. Transient absorption spectrum, visible part, recorded 50 ns after flash photolysis of references **7b** (•••), **7c** (− − −), and **7d** (—) (~5.0×10^{-5} M) at 355 nm in deoxygenated toluene illustrating the oligomer triplet−triplet features (λ_{max} at 545 (**7d**), 580 (**7c**), and 630 nm (**7b**)).

varying between 0.9 and 4.5 mM, were used to quench the transient absorptions, from which we derived bimolecular rate constants of 2.5×10^9, 3.1×10^9, and 2.9×10^9 M^{-1} s^{-1} for **7b**, **7c**, and **7d**, respectively, see Figure 4. In analogy to previous studies, this intermolecular reaction is attributed to the photosensitization of cytotoxic singlet oxygen.

Considering a potential electron transfer scenario between the photoexcited oligomer donors and the electron-accepting fullerene, it was deemed necessary to characterize the spectral features of the one-electron oxidized products of the oligomer references **7a**−**d**. To do so, a complementary set of pulse radiolytic oxidation experiments was carried out. This technique was chosen since it is known to be one of the most powerful

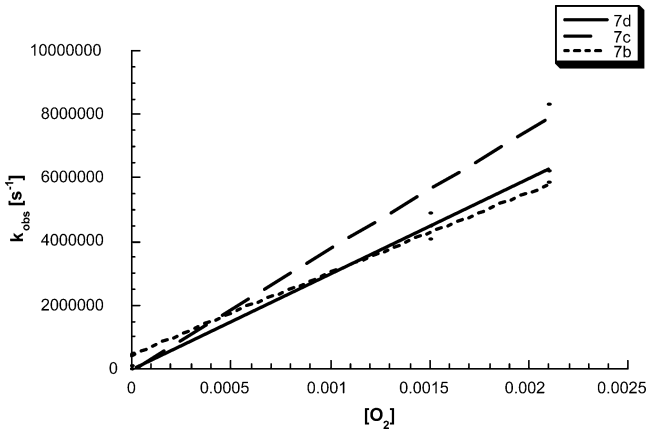

Figure 4. Determination of bimolecular quenching rate constants for the triplet excited states of **7b** (•••), **7c** (− − −), and **7d** (—) with molecular oxygen.

tools to investigate reactive intermediates, evolving from the selective one-electron transfer, for example, to $[CH_2Cl_2]^{\bullet+}$ and $^{\bullet}OOCH_2Cl$/$^{\bullet}OOCHCl_2$ peroxyl radicals in oxygenated dichloromethane solutions. The initial product of solvent ionization (i.e., $[CH_2Cl_2]^{\bullet+}$) and the resulting radicals (i.e., $^{\bullet}OOCHCl_2$ and $^{\bullet}OOCH_2Cl$) are all strong oxidants[14] and are expected to provide the means for the rapid oxidation of the conjugated π-systems. Under aerobic conditions, pulse radiolysis of the tested references led to differential absorption spectra, which are characterized by intense ground-state bleaching around 400 nm, a region that is dominated by the strong ground-state absorption of the oligomer moieties (Figure 5a−c; absorption time profiles are shown in Figure 6). This suggests consumption of **7a**−**d** as a result of a reaction with $^{\bullet}OOCH_2Cl$ and $^{\bullet}OOCHCl_2$ radicals. In addition, new maxima were noted typically 100 μs after the electron pulse in the 600−700 nm region. Importantly, the bleaching kinetics (400 nm) and the grow-in kinetics (600−700 nm) resemble each other very well. Therefore, on the basis of this spectroscopic and kinetic evidence, the underlying reaction is ascribed to a one-electron oxidation process of the conjugated π-systems, yielding π-radical cations.

The rate constants, as determined from a concentration dependence of the substrates ((~0.05−1.0) $\times$ 10^{-4} M^{-1}, not shown) for the bimolecular charge shift reactions from the $^{\bullet}OOCH_2Cl$ and $^{\bullet}OOCHCl_2$ radicals to **7c** and **7d** are ~0.5 $\times$ 10^8 M^{-1} s^{-1} in reasonable agreement with the oxidation strength of these radical species. Only, **7a**, due to its unfavorably shifted oxidation potential (E_{ox} = 1.41 V), could not be oxidized with these radicals; instead, 1,5-dihexyloxynaphthalene reacted only with the short-lived but highly reactive $[CH_2Cl_2]^{\bullet+}$.

Fullerene Reference. Fulleropyrrolidines[15] display three major absorption bands in the ultraviolet region at 220, 265, and 330 nm with extinction coefficients on the order of 100 000 M^{-1} cm^{-1}. In addition, a series of much weaker features are found throughout the visible and near-infrared spectral region. Hereby, the spectroscopically important 0−*0 transition, which char-

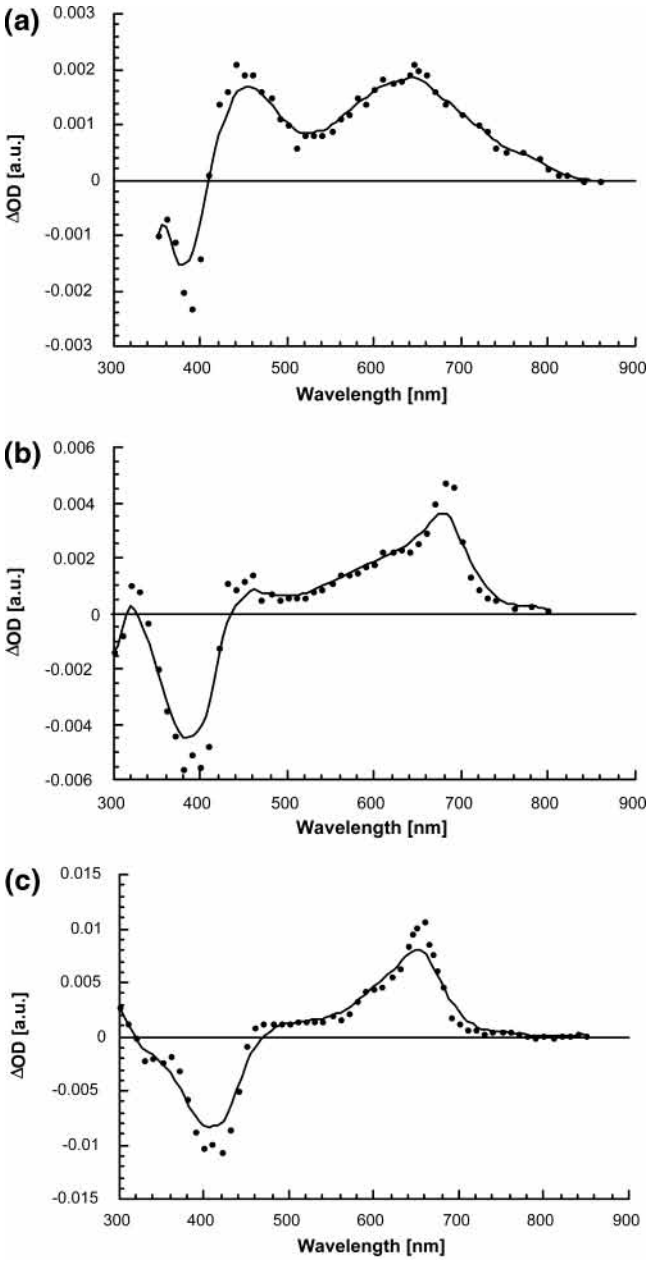

Figure 5. Transient absorption spectrum, visible−near-infrared part, recorded 200 μs after pulse radiolytic oxidation of **7b** (a), **7c** (b), and **7d** (c) ($\sim$1.0 $\times$ 10^{-4} M) in oxygenated dichloromethane solutions illustrating the oligomer π−radical cation features (λ_{max} at 640 (**7b**), 680 (**7c**), and 660 nm (**7d**)). The lines represent weighted fits of the experimental data points.

acterizes the energy gap between the lowest vibrational state of the singlet ground and that of the singlet excited state, is located at 690 nm.

In the excited state, fulleropyrrolidines show well-resolved fluorescence spectra with peaks at 703, 716, 724 (sh), 739, 754, 783, and 796 nm (sh) in a frozen matrix, such as a methylcyclohexane glass. At room temperature, besides a small red shift of the emission maxima relative to the low-temperature measurements, a weak solvent dependence was noted. Specifically, the *0−0 transition shifts progressively from 713 to 719 nm with increasing solvent polarity (i.e., toluene → dimethylformamide), while the emission intensity remains unaffected. The highly constrained carbon network in fullerenes inhibits vibrational motion, C−C bond elongation, or even changes of the dipole moment and, therefore, results in the minor Stokes shifts

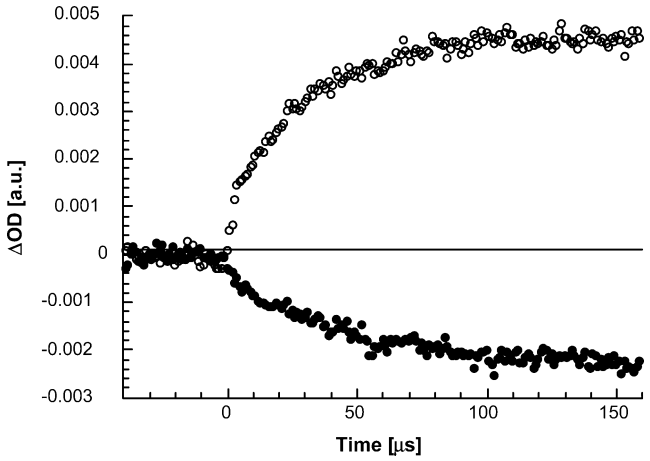

Figure 6. Absorption time profiles reflecting the pulse radiolytic oxidation experiments of **7d** as recorded at 690 nm (○) and at 400 nm (●).

as an energetic measure for the difference between ground and excited-state coordinates.

Pumping light into the fullerene ground state with a short 355 nm laser pulse (18 ps) leads to the population of the singlet excited state. The lifetime of this intermediate state is relatively short since, once formed, the lowest vibrational state of the singlet excited state undergoes a rapid and quantitative intersystem crossing to the energetically lower lying triplet. In the currently employed fullerene reference, this ISC takes place with a time constant of 7.4 $\times$ 10^8 s^{-1}, governed by a large spin−orbit coupling. This leads to much faster dynamics than those noticed in most two-dimensional aromatic hydrocarbons. Spectral characteristics of the main excited states for the selected fullerene reference comprise transient absorption in the near-infrared with characteristic maxima around 900 and 700 nm for the singlet and triplet excited state, respectively.

As far as the fullerene triplet lifetime is concerned, a clean monoexponential recovery of the singlet ground state follows at low fullerene concentration and low laser power, affording a triplet lifetime of ca. 100 μs. However, under our standard conditions in condensed media, triplet lifetimes of ca. 20 μs are obtained. This can be rationalized in terms of efficient (i) triplet−triplet annihilation and (ii) triplet-ground-state quenching processes, which impact the fullerene triplet kinetics, for example, at high fullerene concentrations and high laser power.

The spectral features of the fullerene π-radical anion, the one-electron reduced product of the electron acceptor moiety, are well-known. In particular, two prominent maxima, one in the visible around 400 nm ($\epsilon_{400nm} \approx 15\,000$ M^{-1} cm^{-1}) and one in the near-infrared at 1000 nm ($\epsilon_{1000nm} \approx 8000$ M^{-1} cm^{-1}), are the characteristic fingerprints of a reduced fulleropyrrolidine.[16]

In summary, the above features, which are linked to the ground, excited, oxidized, and reduced states of the oligomer references **7a−d**, are convenient markers for the below-described intramolecular transfer reactions. It is expected that the use of these probes will serve as a reference data set for the covalently linked fullerene-containing triads **5a−d**.

Triads. *Absorption Spectra.* Significant deviations were noted between the absorption spectra of triads **5a−d** in dichloromethane solutions and the simple superimpositions of the spectra of the component chromophores making up triads **5a−d** (i.e., C_{60} and the conjugated π-systems, Figure 7). This trend is not limited to dichloromethane; a similar lack of superimposition of the relative component spectra was found in toluene, THF, and benzonitrile solutions. Consequently, we propose the notion

TABLE 3: Photophysical Data of Fullerene-Based Triads (5)[a]

compd	8	5a	5b	5c	5d
fluorescence maxima [nm]	715,[b] 715[c]	715,[b] 715[c]	715,[b] 715[c]	715,[b] 715[c]	715,[b] 715[c]
Φ_{fluor} oligomer (toluene)		5.3×10^{-3} [d]	3.4×10^{-3} [e]	4.1×10^{-4} [e]	4.1×10^{-4} [e]
$\Phi_{FLUOR.}$ Oligomer (THF)		4.3×10^{-3} [d]	4.5×10^{-3} [e]	3.6×10^{-4} [e]	3.1×10^{-4} [e]
Φ_{fluor} fullerene (toluene)	6.0×10^{-4}	4.52×10^{-4}	4.09×10^{-4} [e]	4.82×10^{-4} [e]	5.4×10^{-4} [e]
Φ_{fluor} fullerene (THF)	6.0×10^{-4}	3.99×10^{-4}	3.07×10^{-4} [e]	2.11×10^{-4} [e]	0.39×10^{-4} [e]
k_{energy} [s^{-1}] (toluene)		[f]	2.3×10^{11}	1.0×10^{12}	7.2×10^{11}
ISC (toluene) [ns]	1.35	1.22	1.19	1.28	1.19
ISC (BZCN) [ns]	1.39	1.16	1.26	1.21	
τ_{fluor} fullerene (BZCN) [ns]	1.38	1.44	1.23	1.41	0.86
triplet maxima [nm]	700	700	700	700	700
$\Phi_{triplet}$ fullerene (toluene)	0.98	0.72	0.68	0.70	0.82
$\Phi_{triplet}$ fullerene (THF)	0.95	0.60	0.46	0.39	radical pair
$\Phi_{triplet}$ fullerene (BZCN)	0.95	0.51	0.43	0.29	radical pair

[a] For details on the data determination, see Experimental Section. [b] In toluene. [c] In THF. [d] Excitation wavelength = 334 nm. [e] Excitation wavelength = 410 nm. [f] No reference available.

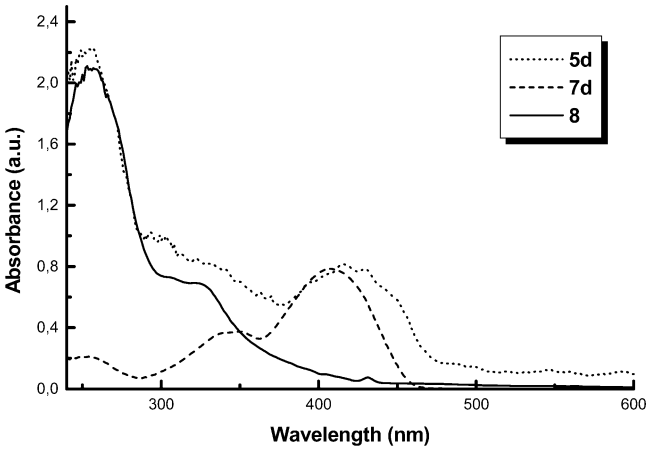

Figure 7. Absorption spectra of triad **5d**, together with those of reference compounds **7d** and **8**.

that some electronic perturbation within the triad structures exists. This may stem from linking the redox and photoactive blocks to each other such that notable coupling exists between the individual chromophores in their ground-state configuration.

Emission Spectra. To shed light onto the extent of the electronic interaction between the conjugated π-systems and the fullerene fragments in the excited state, emission measurements were carried out with triads **5a**−**d**. Additionally, they were compared to those of the respective model oligomer compounds **7a**−**d**. As a general feature (see Table 3), the nearly unit quantum yields of emission, seen in the reference oligomers (i.e., between 54% and 72%), are quenched in all triads (i.e., between 0.03% and 0.5%). An illustration is given in Figure 8. Despite the weak fluorescence, the emission patterns of the conjugated π-systems remain unchanged and are not affected noticeably by the presence of the attached fullerene cores.

The fluorescence data give rise to a number of important trends. First and far most important, even in nonpolar toluene, the oligomer emission in the triads is nearly quantitatively quenched. Despite the near exclusive excitation of the oligomer fragment (i.e., ~90%), the familiar fullerene fluorescence spectrum appears in the near-infrared with a strong *0−0 emission at 715 nm.[15] Further evidence for the fullerene emission came from experiments that make use of the heavy ion effect for a controlled acceleration of the ISC process between the fullerene singlet and triplet excited states. Addition of ethyl iodide, a heavy atom provider, led to a complete cancellation of this fullerene fluorescence, and instead, the characteristic 824 nm fullerene phosphorescence was detected.[10,17] The dual emission recorded for triads **5a**−**d**, namely,

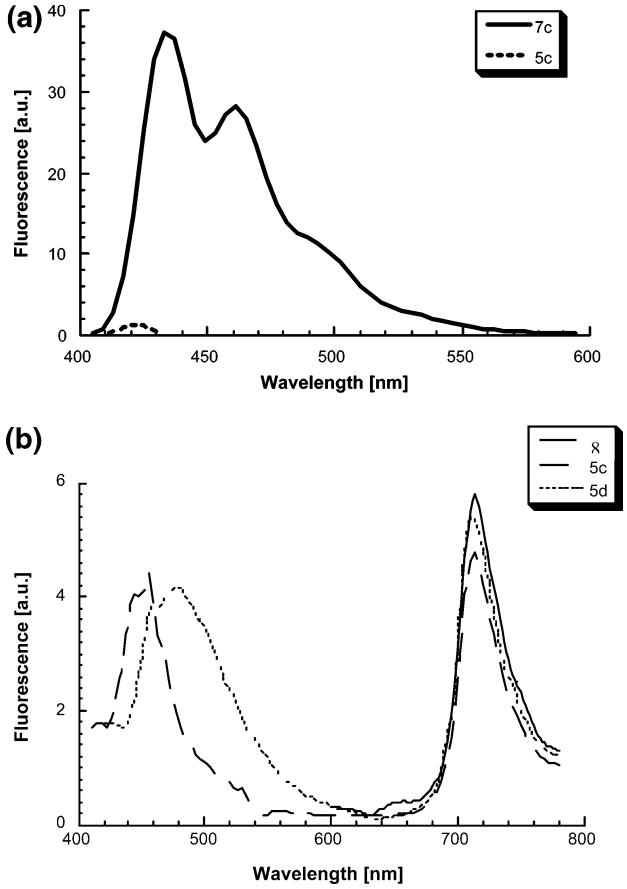

Figure 8. Emission spectra of (a) reference **7c** and triad **5c** and **(**b**)** fullerene reference **8** and triads **5c** and **5d** in toluene with matching absorption at the 410 nm excitation wavelength (i.e., $OD_{410\ nm} = 0.5$).

that of the oligomers and that of the fullerene fragments, suggest an efficient transduction of singlet excited-state energy.

To test the mechanism by which the fullerene emission is generated, an excitation spectrum of the 715 nm emission was recorded − see Figure 9. Typical experiments reveal that the excitation spectra of triads **5a**−**d** were reasonable matches of those analogues recorded for oligomer models **7a**−**d**. In addition, the maxima also resemble the ground-state transitions. Taking these evidences into account, we reach the important conclusion that the origin of excited-state energy is unquestionably that of the conjugated π-systems, which prompts to an efficient intramolecular transfer of singlet excited-state energy from the photoexcited oligomer to the covalently linked C_{60}.

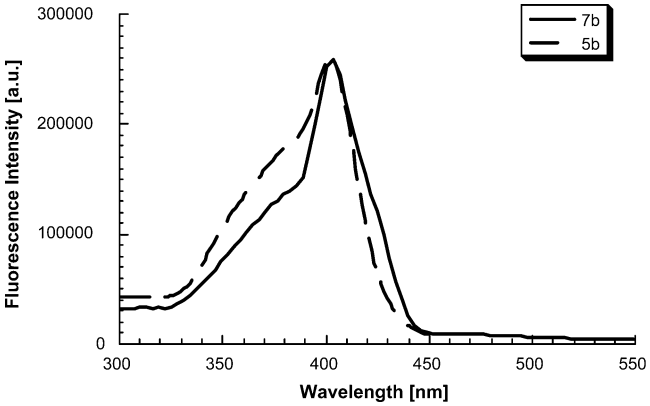

Figure 9. Excitation spectra (normalized to exhibit matching signals around 400 nm) of dyad **5b** in toluene (−••) and reference **7b** in toluene (—), monitoring the fullerene emission at 715 nm and oligomer emission at 430 nm, respectively.

The rate constant (k) of the intramolecular singlet−singlet energy transfer in the investigated triads **5b**−**d** can be calculated according to the following expression:[5f]

$$k = [\Phi(\mathbf{7a}-\mathbf{d}) - \Phi(\mathbf{5b}-\mathbf{d})]/[\tau(\mathbf{7a}-\mathbf{d})\Phi(\mathbf{5b}-\mathbf{d})] \quad (1)$$

In eq 1, Φ and τ denote the fluorescence quantum yields and the fluorescence lifetime of photoexcited oligomer models **7a**−**d**. The determined rates ($\sim 10^{12}$ s^{-1}) infer a strong coupling between the two moieties.

With the help of a fullerene standard, the fullerene fluorescence quantum yields were deduced in triads **5a**−**d**. In toluene, Φ-values nearly approach that measured for the reference, 6.0×10^{-4}, and do not vary with excitation wavelength. It is interesting to note that the energy transfer appears to occur more efficiently at smaller energy gaps, that is, the difference between the singlet excited state of the oligomer and that of the fullerene core, than at larger ones. A possible rationale involves as a consequence a weaker spectral overlap at larger energy gaps, for instance, between photoexcited **7a** and ground-state **8** relative to the analogous correlation gathered for the **7c**−**8** and **7d**−**8** couples.

The emission of the conjugated π-system in triads **5a**−**d** is in THF, similar to the trends discussed for toluene, strongly quenched in relation to the emission of reference oligomers **7a**−**d** with quantum yields that are somewhat smaller than those in toluene. The emission of the fullerene, on the other hand, differs substantially from this trend. Considering the quantum yields in the dihexylnaphthalene-based systems, the THF values diverge moderately by ~10% and ~22% from the corresponding toluene values for the monomeric and trimeric dihexyloxynaphthalene, respectively. Larger effects were seen in the systems that have thiophene building blocks incorporated. The differences, for example, between toluene and THF solutions were 57% (dihexyloxynaphthalene/thiophene) and 95% (1,4-dihexyloxybenzene/thiophene).

The aforementioned trends let us assume that yet another second pathway competes with the energy transfer in the overall deactivation of the photoexcited oligomers. A highly exothermic electron transfer scenario should be considered. This assumption is primarily based on the driving force dependence ($-\Delta G^{\circ}_{CS}$) for an electron-transfer process. The latter predicts enhanced exothermicity of an electron transfer in polar solvents. Spectroscopic support for the "electron transfer" hypothesis will be provided (vide infra).

The differences in emission quenching arising between the currently studied triads and the previously published dyads are generally very small. Similar quantum yields were noted in all of the dyads and triads sets. This suggests that, at least for aspects concerned with the deactivation of the photoexcited chromophore, utilization of two fullerene moieties instead of just one excludes cooperative effects.

Fluorescence Lifetimes Measurements. At last, we measured the fluorescence lifetimes of triads **5b**−**d** in nonpolar toluene and polar benzonitrile (Table 3). These experiments allowed probing the decay dynamics of the fullerene and conjugated π-systems separately. Therefore, the fluorescence decay was monitored around 430 and 715 nm, relating to the emission of the conjugated π-system and the fullerene moiety, respectively. In general, the fluorescence decay curves were well fitted by a single-exponential decay component. Importantly, the emission of the conjugated π-system around 430 nm is within the 100 ps time resolution of the apparatus in toluene and in benzonitrile. This result is consistent with the steady-state emission (i.e., nearly quantitative fluorescence quenching) and the time-resolved transient absorption measurements (i.e., only photoexcited fullerene characteristics), see below. In contrast, the fluorescence lifetime of the fullerene moiety in toluene and benzonitrile of $\sim 1.3 \pm 0.1$ ns is comparable to that of the fulleropyrrolidine reference. The only exception was seen for the 1,4-dihexyloxybenzene/thiophene based array **5d** in benzonitrile, which showed an accelerated decay of the fullerene fluorescence with a lifetime of 0.86 ns. Considering the ($-\Delta G^{\circ}_{CS}$) in benzonitrile, this acceleration can be plausibly connected to an intramolecular electron transfer evolving from the fullerene singlet excited state. From this, we estimate fluorescence quantum yields, assuming an exclusive fullerene excitation, of 3.7×10^{-4} (**5d**).

Transient Spectroscopy in Toluene. Transient absorption changes, recorded upon 355 nm laser excitation of all investigated triads, reveal broad maxima around 900 nm, which correspond, however, to the fullerene singlet−singlet absorption. After all, this observation does not come surprising, although we predominantly excited the conjugated π-systems, since it confirms the rapid transduction of singlet excited-state energy. Time profiles, taken at various wavelengths, indicate that the fullerene singlet excited state is formed instantaneously and in a single step. The formation dynamics are, however, masked by the apparatus's resolution, and thus, we can only provide an estimate for the intramolecular energy transfer rate constant, $k \geq 5.0 \times 10^{10}$ s^{-1}.

The fullerene singlet excited states are short-lived, since a rapid and quantitative ISC to the triplet manifold takes place. Two maxima located at 360 and 700 nm and a low-energy shoulder around 800 nm characterize the fullerene triplet excited state in triads **5a**−**d**. The photosensitization effect of the conjugated π-system chromophore, acting as an antenna system and transmitting its excited energy to the covalently attached fullerenes, enables the efficient fullerene triplet generation with quantum yields close to unity.

Transient Spectroscopy in Tetrahydrofuran. The results in THF are virtually identical with those presented for toluene involving the same key intermediates in the overall reaction sequence. The picosecond measurements revealed that an efficient singlet−singlet energy transfer, stemming from the originally excited oligomer to the energetically lower-lying fullerene singlet excited state, prevails. The transient absorption changes noted immediately after the laser pulse, which are formed in a single step, match the fullerene singlet−singlet transitions in the near-infrared, similar to those shown in Figure 10.

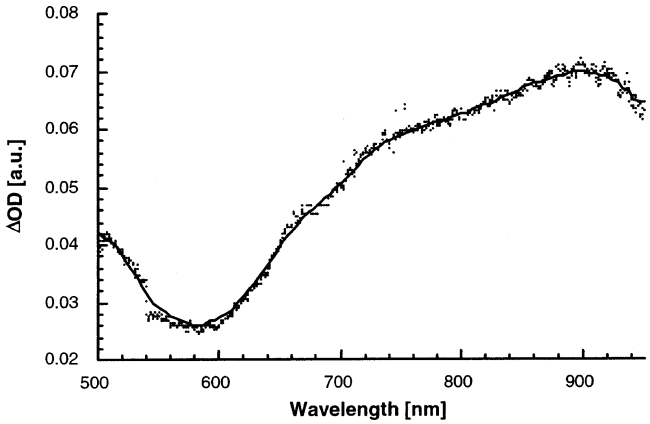

Figure 10. Transient absorption spectrum, visible−near-infrared part, recorded 20 ps after flash photolysis of **5c** ($\sim 5.0 \times 10^{-5}$ M) at 355 nm in deoxygenated toluene indicating the fullerene singlet−singlet features ($\lambda_{max} = 900$ nm).

Likewise the fullerene ISC kinetics in THF are on the order of 7.5×10^8 s^{-1}, affording accordingly the energetically lower lying triplet excited state. Interestingly, the quantum yields of the latter are markedly reduced relative to those in toluene, despite the same absorption ratio between the fullerene and oligomer moieties. The lower Φ-values, especially in polar solvents, correlate with larger free energy changes ($-\Delta G^\circ_{CS}$) for the associated electron transfer (Table 4, details can be found in the Supporting Information) and, in turn, indicate that an increasing contribution of electron transfer exists. The driving force dependence ($-\Delta G^\circ_{CR}$; $-\Delta G^\circ_{CS}$) and thermodynamic parameters (λ; $\Delta G^{\ddagger}_{CS}$), as listed in Table 4, support the notion. For example, the $-\Delta G^\circ_{CS}$ values increase with solvent polarity, while the $\Delta G^{\ddagger}_{CS}$ values decrease simultaneously.

Direct evidence for the electron transfer product, could, however, only be confirmed for **5d**. Hereby, the strongly overlapping spectra of the fullerene triplet ($\lambda_{max} = 700$ nm) and of the π-radical cation (**7d**; $\lambda_{max} = 690$ nm) between 600 and 800 nm render an analysis of the far-visible region rather ambiguous. This imposes a definite disadvantage to the spectral analysis by just limiting it to the fullerene π-radical anion fingerprint around 1000 nm.

Transient Spectroscopy in Benzonitrile. Electron transfer, as the sole deactivation mechanism, was only found for **5d**, in which the low oxidation potential of the 1,4-dihexyloxybenzene/thiophene donor guarantees that the energy of the charge-separated state lies below that of the fullerene singlet excited state. In line with this, the immediate occurrence of a 690 nm band, which we assign to the π-radical cation of the oligomer (vide infra), supports the electron-transfer mechanism, see Figures 11 and 12.

Raising the energy of the charge-separated state in **5c** (i.e., 1,4-dihexyloxynaphthalene/thiophene), close to that of the fullerene singlet, led again to two photoproducts, that is, electron transfer and energy transfer. Electron transfer was inferred on the basis of the instantaneously produced 700 nm maximum, while the presence of the 900 nm absorption and an ISC rate of 7.1×10^8 s^{-1} are clear attributes connected with an energy transfer product.

Quite differently, the picosecond changes of **5a** and **5b** are overshadowed by the dominance of the fullerene photophysics, that is, formation of the singlet excited state followed by the subsequent ISC. No spectral evidence of the π-radical cation was found that would testify to an electron transfer mechanism. A plausible explanation for this observation is that in the dihexyloxynaphthalene systems the energies of the charge-separated state are unfavorably raised, passing that of the fullerene singlet.

TABLE 4: Driving Force Dependence ($-\Delta G^\circ_{CR}$; $-\Delta G^\circ_{CS}$) and Thermodynamic Parameters (λ; $\Delta G^{\ddagger}_{CS}$) for Intramolecular Electron Transfer Events in Fullerene-Based Triads (5)

compd	5a	5b	5c	5d
radius donor, R_+ [Å]	2.45	11.35	8.5	7.5
donor−acceptor separation, R_{D-A} [Å]	8.2	16.0	12.8	11.1
$-\Delta G^\circ_{CR}$[a] (toluene) [eV]	2.89	2.46	2.29	2.02
$-\Delta G^\circ_{CR}$[a] (THF) [eV]	2.03	2.04	1.86	1.62
$-\Delta G^\circ_{CR}$[a] (BZCN) [eV]	1.75	1.90	1.74	1.49
	oligomer			
$-\Delta G^\circ_{CS}$[b] (toluene) [eV]	0.65	0.43	0.62	0.68
$-\Delta G^\circ_{CS}$[b] (THF) [eV]	1.51	0.85	1.05	1.08
$-\Delta G^\circ_{CS}$[b] (BZCN) [eV]	1.79	0.99	1.17	1.21
	fullerene			
$-\Delta G^\circ_{CS}$[b] (toluene) [eV]	−1.13	−0.70	−0.53	−0.26
$-\Delta G^\circ_{CS}$[b] (THF) [eV]	−0.27	−0.28	−0.10	0.14
$-\Delta G^\circ_{CS}$[b] (BZCN) [eV]	0.01	−0.14	0.02	0.27
λ[c] (toluene) [eV]	0.39	0.34	0.34	0.34
λ[c] (THF) [eV]	1.43	0.85	0.85	0.82
λ[c] (BZCN) [eV]	1.47	0.87	0.86	0.84
	oligomer			
$\Delta G^{\ddagger}_{CS}$[d] (toluene) [eV]	0.046	0.006	0.06	0.09
$\Delta G^{\ddagger}_{CS}$[d] (THF) [eV]	0.001	0	0.012	0.03
$\Delta G^{\ddagger}_{CS}$[d] (BZCN) [eV]	0.017	0.004	0.027	0.05
	fullerene			
$\Delta G^{\ddagger}_{CS}$[d] (THF) [eV]				0.14
$\Delta G^{\ddagger}_{CS}$[d] (BZCN) [eV]			0.21	0.09

[a] Determined from the following relations: $-\Delta G^\circ_{CR} = E_{1/2}(D^{\bullet+}/D) - E_{1/2}(A/A^{\bullet-}) + \Delta G_S$; $\Delta G_S = e^2/(4\pi\epsilon_0)(1/(2R_+)) + 1/(2R_-) - 1/R_{D-A}(1/\epsilon_S) - 1/(2R_+) + 1/(2R_-)(1/(\epsilon R))$; $E_{1/2}(D^{\bullet+}/D)$ = oxidation potential of the respective donor (see Table 1); $E_{1/2}(A/A^{\bullet-})$ = reduction potential of acceptor (see Table 1); R_+ = radius donor (determined by molecular modeling (MM+) as half of the molecule's length, see top of this table); R_{D-A} = donor−acceptor separation (determined by molecular modeling (MM+), assuming that the charges are located at the centers of the π-conjugated and fullerene moieties, see top of this table); R_- = radius acceptor (4.4 Å); ϵ_s = solvent dielectric constant (toluene = 2.39; THF = 7.6; benzonitrile = 24.8); ϵ_R = solvent dielectric constant for electrochemical measurements (9.412). [b] Determined from the following relation: $-\Delta G^\circ_{CS} = \Delta E_{0-0} - (-\Delta G_{CR})$; ΔE_{0-0} = excited-state energy of the chromophore in the triads. [c] Determined from the following relations: $\lambda = \lambda_i + \lambda_S$; $\lambda_S = e^2/(4\pi\epsilon_0)(1/(2R_+)) + 1/(2R_-) - 1/R_{D-A}(1/n^2) + 1/\epsilon_S$; λ_i = internal reorganization energy (0.3 eV); λ_S = solvent reorganization energy; n = solvent refractive index (toluene = 1.496; THF = 1.407; benzonitrile = 1.528). [d] determined from the following relation: $\Delta G^{\ddagger}_{CS} = (\Delta G_{CS} + \lambda^2)/(4\lambda)$; $\Delta G^{\ddagger}$ = Gibbs activation energy.

In the context of confirming the electron-transfer mechanism, the strong and broad triplet−triplet absorption leads to certain complications. Straightforward is the picture only in the 1,4-dihexyloxybenzene/thiophene based array (**5d**): full spectral characterization of the charge-separated state was accomplished directly with the help of complementary nanosecond measurements. For example, photolysis of a benzonitrile solution of **5d** led to maxima at 1000 and 680 nm. On the basis of a spectral comparison, we ascribe the former band to the fullerene π-radical anion, while the latter reveals the broadened characteristics of the 1,4-dihexyloxybenzene/thiophene π-radical cation **7d**. In accordance with these results, we propose the occurrence of a photoinduced electron transfer, evolving from the singlet excited state of the chromophore (i.e., conjugated π-system) to the electron-accepting fullerene and, in turn, creating the charge-separated radical pair.

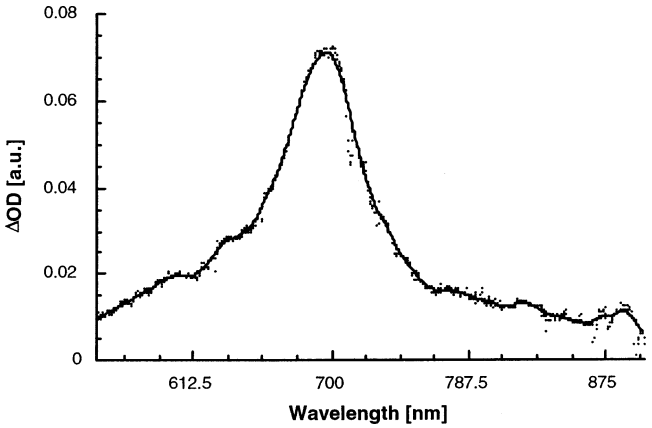

Figure 11. Transient absorption spectrum, visible−near-infrared part, recorded 20 ps after flash photolysis of **5d** (2.0×10^{-5} M) at 355 nm in deoxygenated benzonitrile indicating the oligomer π−radical cation features ($\lambda_{max} \approx 700$).

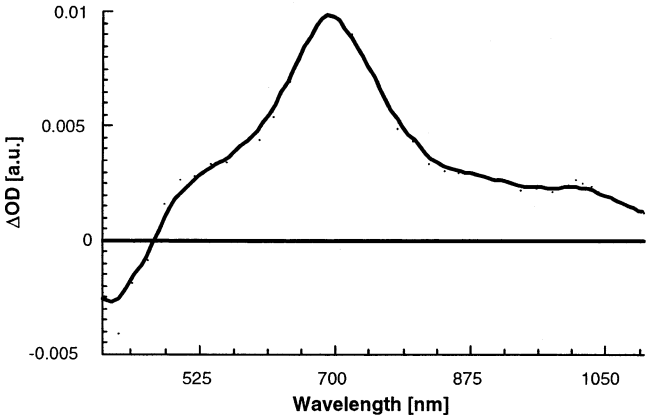

Figure 12. Transient absorption spectrum, visible−near-infrared part, recorded 50 ns after flash photolysis of dyad **5d** (2.0×10^{-5} M) at 355 nm in deoxygenated benzonitrile solutions, indicating the charge-separated radical pair features (λ_{max} at 680 and 1000 nm).

CHART 4

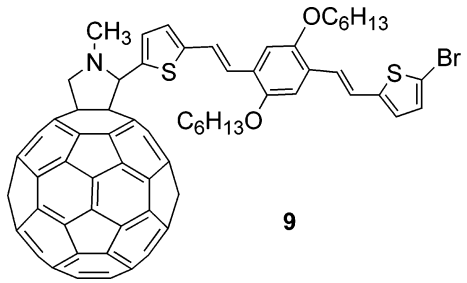

9

Both fingerprints allowed us to determine the lifetime of the charge-separated states. The decay curves were well fitted by a single-exponential decay component with lifetimes that are on the order of a microsecond−0.98 μs (THF), 1.84 μs (benzonitrile). One of the most striking observations transpires upon comparing the charge recombination kinetics in the dyad (**9**, Chart 4)[4b] versus triad ensemble (**5d**). The charge-separated states in **5d** (1.84 μs, benzonitrile) are appreciably longer lived than those in **9** (1.37 μs, benzonitrile). In line with the enhanced stabilization of the charge-separated state, higher quantum yields of charge separation were also found in the triad system. In benzonitrile, the triad shows a 67% enhanced quantum yield. This clearly points to cooperative effects evolving from the two fullerene moieties.

Activation Barrier ($\Delta G^{\ddagger}_{CS}$) and Electronic Coupling Matrix Element (V). In summary, only the favorable thermodynamics in **5d** secure the activation of the electron-transfer channel. However, this takes place regardless of the photoexcited precursor state, namely, either the fullerene or the oligomer. To analyze these electron transfer reactions in light of the relevant thermodynamic parameters and to gain further insight into the associated kinetics, the semiclassical Marcus equations were employed.[18] In its final instance, this processing enables evaluating the reorganization energy (λ), the activation barrier for the electron-transfer reaction ($\Delta G^{\ddagger}_{CS}$), and the electronic coupling matrix element (**V**) (see, for details, footnotes to Tables 4 and 5).

To obtain the important $-\Delta G^{\ddagger}_{CS}$ and **V** values, the reorganization energy (λ) was first computed in view of its internal (λ_i) and solvent contributions (λ_s). The former value (λ_i), which relates primarily to the structural differences between the reactant and product, was taken from the literature as 0.3 eV.[10] By contrast, the λ_s values, the difference in orientation and polarization of solvent molecules between the initial and final states, were evaluated in reference to the Born−Hush approach (see footnotes to Table 4). Considering the above-estimated free energy changes ($-\Delta G^{\circ}_{CS}$) in relation to the λ values (0.84 ± 0.01), we reach the important conclusion that the electron-transfer reactions evolving from the photoexcited fullerene moiety and those from the photoexcited 1,4-dihexyloxybenzene/thiophene moiety are in the "Marcus-normal" (i.e., $-\Delta G^{\circ}_{CS} < \lambda$) and "Marcus-inverted" region (i.e., $-\Delta G^{\circ}_{CS} > \lambda$), respectively. Most importantly, the small activation barriers ($\Delta G^{\ddagger}_{CS}$) ranging between 0.05 and 0.09 eV for the 1,4-dihexyloxybenzene/thiophene-based arrays infer that these transfer processes occur under nearly optimal conditions, that is, in close vicinity to the top region of the "Marcus curve" (i.e., $-\Delta G^{\circ}_{CS} \approx \lambda$).

From a closer inspection, the electronic coupling matrix elements (**V**) were determined as $\sim$250 cm^{-1} in benzonitrile and $\sim$140 cm^{-1} in THF, respectively (Table 5). Since the estimated $-\Delta G^{\ddagger}_{CS}$ and λ values are in reasonable agreement with those reported in various donor−acceptor ensembles,[19] it confirms unequivocally that the strong coupling matrices are the main cause responsible for the rapid electron-transfer processes. This rationale is in accord with the perturbation of the ground-state spectra and the oxidation potential, being both sensitive probes for the extent of electronic interactions.

Nevertheless, a final note should address the quite different **V** values, depending on from which end the electron transfer is initiated, namely, either from the photoexcited fullerene or the photoexcited oligomer. Larger **V** values in case of the latter demonstrates that the chosen oligomer moiety (**7d**) is quite susceptible to electronic perturbations—see differences between absorption and emission spectra. This is limited not only to effects originating from the substitution pattern, but, more crucially, to the electron-withdrawing nature of the appendage (i.e., fullerene). By contrast, the fullerene moiety evidently lacks this amendment, an effect that stems from the pronounced possibility for charge and energy delocalization within the fullerene framework, minimizing and likewise compensating vibrational or electronic differences.

Conclusions

In summary, we have synthesized a series of C_{60}-based triads in which the two C_{60} units are connected through a π-conjugated electroactive oligomer by using a 2-fold 1,3-dipolar cycloaddition reaction. Variation of the arylene units forming the π-conjugated oligomer (naphthalene, benzene, and thiophene)

TABLE 5: Rate Constants (Forward and Backward) and Electronic Coupling Element (V) for the Electron Transfer in 9 and 5d at Room Temperature

	$^1(C_{60})-$oligomer		$C_{60}-{}^1$(oligomer)				$(C_{60})^{\bullet-}-(\text{oligomer})^{\bullet+}$	
	bzcn		bzcn		THF		bzcn	thf
compd	k_{et}[a] [s^{-1}]	**V**[c] [cm^{-1}]	k_{et}[b] [s^{-1}]	**V**[c] [cm^{-1}]	k_{et} [s^{-1}]	**V**[c] [cm^{-1}]	k_{bet} [s^{-1}]	k_{bet} [s^{-1}]
9	1.0×10^9	15	9.5×10^{11}	248	8.2×10^{11}	133	7.2×10^5	1.4×10^6
5d	1.2×10^9	16	1.1×10^{12}	267	9.5×10^{11}	143	5.4×10^5	1.0×10^6

[a] Determined from the fullerene fluorescence lifetimes (see Table 3) and the following relation: $k_{et} = 1/\tau(\mathbf{8}) - 1/\tau(\mathbf{9},\mathbf{5d})$. [b] Determined from the oligomer fluorescence quantum yields in benzonitrile: **9**, $\Phi_{fluor} = 3.1 \times 10^{-4}$; **5d**, $\Phi_{fluor} = 2.8 \times 10^{-4}$. [c] Determined from the following relation for a nonadiabatic electron transfer: $k_{et} = [4\pi^3/(h^2\lambda k_B T)]^{1/2}\mathbf{V}^2 \exp[-\Delta G^{\ddagger}/(k_B T)]$; h = Planck constant; k_B = Boltzmann constant (0.025 eV at 298 K); T = absolute temperature (298 K); λ = reorganization energy (see Table 4); $\Delta G^{\ddagger}$ = Gibbs activation energy (see Table 4).

results in control of the absorption wavelength and the oxidation potential values for the oligomeric donor moiety.

The cyclic voltammetry measurements carried out at room temperature reveal the amphoteric redox behavior of these triads and some electronic interaction between the donor oligomer moiety and the accepting fullerene in the ground state.

Photophysical measurements demonstrated that generally an intramolecular electron transfer competes with the dominant singlet−singlet energy transfer in triads **5a**−**d**. This observation is in good agreement with the thermodynamics of the investigated systems that predict a highly exergonic energy transfer and a much less exergonic electron transfer reaction. By control of the solvent polarity and the structure of fluorescent π-conjugated systems, the outcome of an ultrarapid intramolecular deactivation of a photoexcited oligomer core was successfully shifted from an all energy transfer to an all electron transfer scenario. Small activation barriers ($\Delta G^{\ddagger}_{CS}$) and small electronic coupling matrix elements (**V**) ensure rapid intramolecular transfer processes.

The differences in electron/energy transfer quenching arising between the currently studied triads (i.e., $C_{60}-$oligomer$-C_{60}$) and the previously published dyads (i.e., $C_{60}-$oligomer) are generally very small. Still, in terms of stabilizing the product and enhancing the yield of charge separation, comparison with previously reported analogues containing only a single fullerene unit (i.e., dyad) shows that particular benefits were noted by attaching two fullerene cores (i.e., triad) to the oligomeric structure. In benzonitrile, for example, the triad system shows a 67% enhanced quantum yield. This clearly points to cooperative effects evolving from both fullerene moieties.

Experimental Section

Picosecond Laser Flash Photolysis. Picosecond laser flash photolysis experiments were carried out with 355-nm laser pulses from a mode-locked, Q-switched Quantel YG-501 DP Nd:YAG laser system (pulse width 18 ps, 2−3 mJ/pulse). The white continuum picosecond probe pulse was generated by passing the fundamental output through a D_2O/H_2O solution. The excitation and the probe was fed to a spectrograph (HR-320, ISDA Instruments, Inc.) with fiber optic cables and was analyzed with a dual diode array detector (Princeton Instruments, Inc.) interfaced with an IBM-AT computer. The details of the experimental set up and its operation have been described elsewhere.[20]

Nanosecond Laser Flash Photolysis. These experiments were performed with laser pulses from a Molectron UV-400 nitrogen laser system (337.1 nm, 8 ns pulse width, 1 mJ/pulse). The photomultiplier output was digitized with a Tektronix 7912 AD programmable digitizer. A typical experiment consisted of 5−10 replicate pulses per measurement. The averaged signal was processed with an LSI-11 microprocessor interfaced with a VAX-370 computer. Details of the experimental set up can be found elsewhere.[20] Intersystem crossing rates were determined by averaging the singlet−singlet decay and triplet−triplet growth dynamics.

Pulse Radiolysis. Pulse radiolysis experiments were performed by utilizing 50-ns pulses of 8 MeV electrons from a model TB-8/16-1S electron linear accelerator. Basic details of the equipment and the data analysis have been described elsewhere.[21] Dosimetry was based on the oxidation of SCN^- to $(SCN)_2^{\bullet-}$, which in aqueous, N_2O-saturated solutions takes place with $G = 6$ (G denotes the number of species per 100 eV or the approximate micromolar concentration per 10 J of absorbed energy). The radical concentration generated per pulse amounts to 1−3 μM for all of the systems investigated in this study.

Time-Resolved Emission. Fluorescence lifetimes were measured with a Laser Strobe fluorescence lifetime spectrometer (Photon Technology International) with 337 nm laser pulses from a nitrogen laser fiber-coupled to a lens-based T-formal sample compartment equipped with a stroboscopic detector. Details of the Laser Strobe systems are described on the manufactures web site, http://www.pti-nj.com.

Steady-State Emission. Emission and excitation spectra were recorded with a SLM 8100 spectrofluorometer. Fluorescence spectra were measured at room temperature. A 400 or 600 nm long-pass filter in the emission path was used to eliminate the interference from the solvent and stray light for recording the oligomer and fullerene fluorescence, respectively. Fluorescence quantum yields were determined via the comparative method, using 9,10-diphenyl anthracene as reference with a quantum yield of 1. No corrections were performed for the fluorescence, but long integration times (20 s) and low increments (0.1 nm) were applied. The slits were 2 and 8 nm, and each spectrum was an average of at least five individual scans.

The quantum yields of the triplet excited states ($\Phi_{TRIPLET}$) were determined by the triplet−triplet energy transfer method using β-carotene as an energy acceptor. The quantum yields of the charge separation were measured using the comparative method. In particular, the strong fullerene triplet−triplet absorption ($\epsilon_{700nm} = 16\,100\ M^{-1}\ cm^{-1}$; $\Phi_{TRIPLET} = 0.98$)[22] served as probe to obtain the quantum yields for the charge-separated state, especially for the fullerene π-radical anion ($\epsilon_{1000nm} = 4700\ M^{-1}\ cm^{-1}$).[23] For all photophysical experiments, an error of 10% must be considered.

Cyclic Voltammetry. Cyclic voltammograms were recorded on a potentiostat/galvanostat equipped with a software electrochemical analysis by using a GCE (glassy carbon) as working electrode, SCE as reference electrode, Bu_4NClO_4 as supporting electrolyte, and dichloromethane as solvent at a scan rate of 200 mV/s.

Melting Points. All melting points were measured with a melting point apparatus and are uncorrected. FTIR spectra were recorded either as KBr pellets or neat film plates. UV−visible spectra were recorded with a spectrophotometer. ^{13}C and ^{1}H NMR spectra were recorded with a 300 MHz for ^{1}H and 75 MHz for ^{13}C spectrometer. Chemical shifts are given as δ values (int. standard, TMS).

Materials. The functionalized π-conjugated systems (**6a**−**d**)[9] and reference compounds (**7a**−**d**,[4b] **8**[10]) were obtained by following previously described synthetic procedures. Sarcosine and [60]fullerene are commercially available and were used without further purification.

Synthesis of Triads (5a−d). *General Procedure.* The respective dialdehyde (0.05 mmol), 72 mg (0.1 mmol) of [60]fullerene, and 0.5 mmol of *N*-methylglicine (sarcosine) were dissolved in 60 mL of toluene, and the mixture was refluxed for 24 h. After this time, the reaction was allowed to reach room temperature; then the solvent was partially vacuum-evaporated, and then the mixture was poured on a silica gel column. The black solid obtained after chromatography (cyclohexane/toluene) was further purified by repetitive centrifugation using methanol and diethyl ether to yield the corresponding dyads as black solids.

*1,5-Dihexyloxy-2,6-bis(N-methyl-3,4-fulleropyrrolydin-2-yl)-naphthalene (**5a**).* By following the above general procedure and using dialdehyde **6a**[9] as the starting material, we obtained 33 mg (35%) of triad **5a**. ^{1}H NMR ($CDCl_3$, 300 MHz) δ 8.14 (d, 2H, J = 9.0 Hz), 7.88 (d, 2H, J = 9.0 Hz), 5.57 (s, 2H), 5.03 (d, 2H, J = 9.3 Hz), 4.34 (d, 2H, J = 9.3 Hz), 4.22−4.15 (m, 4H), 2.85 (s, 6H), 2.05−1.98 (m, 4H), 1.66 (m, 4H), 1.28 (m, 8H), 0.99 (t, 6H). FTIR (KBr, cm^{-1}) 2923, 2850, 2773, 1631, 1459, 1426, 1337, 526. UV−vis (CH_2Cl_2) λ (nm) 236, 248, 262, 314, 328 (sh), 440. MS *m*/*z* (APCI) (%I) 1880 (M^+, 100), 647 (15). Anal. Calcd. for $C_{148}H_{42}N_2O_2 \cdot 3(CH_3OH)$: C, 91.93; H, 2.73; N, 1.42. Found: C, 92.16; H, 3.60; N, 1.48.

*1,5-Dihexyloxy-2,6-bis2′[2-(N-methyl-3,4-fulleropyrrolydin-2-yl-1,5-dihexyloxynaphthalene-2-yl)]vinylnaphthalene (**5b**).* By following the above general procedure and using dialdehyde **6b**[9] as the starting material, we obtained 36 mg (28%) of triad **5b**. ^{1}H NMR ($CDCl_3$, 300 MHz) δ 8.18 (d, 2H, J = 8.9 Hz), 8.00 (d, 2H, J = 8.9 Hz), 7.88 (d, 4H, J = 9.0 Hz), 7.87 (s, 4H), 7.73 (s, 4H), 5.60 (s, 2H), 5.04 (d, 2H, J = 9.4 Hz), 4.34 (d, 2H, J = 9.4 Hz), 4.19 (t, 4H), 4.05 (m, 4H), 2.81 (s, 6H), 2.02 (m, 12H), 1.68 (m, 12H), 1.43 (m, 24H), 0.95 (m, 18H). FTIR (KBr, cm^{-1}) 2921, 2852, 2773, 1628, 1459, 1405, 1335, 1024, 526. UV−vis (CH_2Cl_2) λ (nm) 256, 310 (sh), 330 (sh), 398, 420. MS *m*/*z* (APCI) (%I) 2585 (M^+, 100). Anal. Calcd. for $C_{196}H_{106}N_2O_6 \cdot 2(CH_3OH)$: C, 89.79; H, 4.41; N, 1.05. Found: C, 89.68; H, 5.04; N, 1.17.

*1,5-Dihexyloxy-2,6-bis[5-(N-methyl-3,4-fulleropyrrolydin-2-yl)-2-thienyl]vinylnaphthalene (**5c**).* By following the above general procedure and using dialdehyde **6c**[9] as the starting material, we obtained 27 mg (26%) of triad **5c**. ^{1}H NMR ($CDCl_3$, 300 MHz) δ 7.83 (d, 2H, J = 8.7 Hz), 7.67 (d, 2H, J = 8.7 Hz), 7.41 (d, 2H, J_{trans} = 16.2 Hz), 7.33 (d, 2H, J = 3.6 Hz), 7.28 (d, 2H, J_{trans} = 16.1 Hz), 7.05 (d, 2H, J = 3.6 Hz), 5.17 (s, 2H), 5.01 (d, 2H, J = 9.8 Hz), 4.27 (d, 2H, J = 9.8 Hz), 3.99 (t, 4H), 3.01 (s, 6H), 1.96 (q, 4H), 1.70 (m, 8H), 1.34 (m, 4H), 0.81 (t, 6H). FTIR (KBr, cm^{-1}) 2927, 2854, 1736, 1636, 1467, 1370, 1244, 1027, 955, 526. UV−vis (CH_2Cl_2) λ (nm) 234, 260, 316, 334 (sh), 380 (sh), 426. MS *m*/*z* (APCI) (%I) 2096 (M^+, 100), 720 (50). Anal. Calcd. for $C_{160}H_{50}N_2O_2S_2 \cdot 6(CH_3OH)$: C, 87.14; H, 3.23; N, 1.49; S, 2.79. Found: C, 86.91; H, 2.71; N, 1.49; S, 2.79.

*1,4-Dihexyloxy-2,5-bis[5-(N-methyl-3,4-fulleropyrrolydin-2-yl)-2-thienyl]vinylbenzene(**5d**).* By following the above general procedure and using dialdehyde **6d**[9] as the starting material, we obtained 30 mg (29%) of triad **5d**. ^{1}H NMR ($CDCl_3$, 300 MHz) δ 7.59 (d, 1H, J = 3.9 Hz), 7.41 (d, 2H, J_{trans} = 16.5 Hz), 7.23 (s, 2H), 7.20 (d, 2H, J_{trans} = 16.5 Hz), 7.06 (d, 1H, J = 3.9 Hz), 6.96 (s, 2H), 5.16 (s, 2H), 4.98 (d, 2H, J = 9.3 Hz), 4.27 (d, 2H, J = 9.3 Hz), 4.00 (t, 4H), 3.29 (s, 6H), 1.79 (m, 4H), 1.32 (m, 6H), 0.85 (t, 6H). FTIR (KBr, cm^{-1}) δ 2921, 2851, 2757 526. UV−vis (CH_2Cl_2) λ (nm) 234, 258, 314, 338, 424. MS *m*/*z* (ESI) (%I) 2010 (M^+-SH_2, 12), 1349 (44), 963 (12), 701 (51), 686 (100). Anal. Calcd. for $C_{156}H_{48}N_2O_2S_2 \cdot 2(CH_3OH)$: C, 89.94; H, 2.66; N, 1.33; S, 3.03. Found: C, 89.72; H, 2.74; N, 1.33; S, 2.98.

Acknowledgment. This work has been partially supported by the DGESIC of Spain (Project BQU2002-00855), by the European Comission (Contract JOR3CT980206), and by the Office of Basic Energy Sciences of the U.S. Department of Energy (Contribution No. NDRL-4497 from the Notre Dame Radiation Laboratory). We are also indebted to Centro de Espectroscopía de la UCM.

Supporting Information Available: Details of the thermodynamics calculations. This material is available free of charge via the Internet at http://pubs.acs.org.

References and Notes

(1) (a) Granström, M.; Petritsch, K.; Arias, A. C.; Lux, A.; Andersson, M. R.; Friend, R. H. *Nature* **1998**, *395*, 257. (b) Gao, J.; Yu, G.; Heeger, A. J. *Adv. Mater.* **1998**, *10*, 692. (c) van Hal, P. A.; Christiaans, M. P. T.; Wienk, M. M.; Kroon, J. M.; Janssen, R. A. J. *J. Phys. Chem. B* **1999**, *103*, 4352. (d) Huynh, W. U.; Peng, X.; Alivisatos, A. P. *Adv. Mater.* **1999**, *11*, 923. (e) Halls, J. J. M.; Arias, A. C.; Mackenzie, J. D.; Wu, W.; Inbasekaran, M.; Woo, E. P.; Friend, R. H. *Adv. Mater.* **2000**, *12*, 498. (f) Wallace, G. G.; Dastoor, P. C.; Officer, D. L.; Too, C. O. *Chem. Innovation* **2000**, *30* (1), 14.

(2) (a) Sariciftci, N. S.; Smilowitz, L.; Heeger, A. J.; Wudl, F. *Science* **1992**, *258*, 1474. (b) Sariciftci, N. S. *Prog. Quantum Electron.* **1995**, *19*, 131. (c) Sariciftci, N. S.; Heeger, A. J. In *Handbook of Organic Conductive Molecules and Polymers*; Nalwa, H. S., Ed.; Wiley: New York, 1996.

(3) Yu, G.; Gao, Y.; Hummelen, J. C.; Wudl, F.; Heeger, A. J. *Science* **1995**, *270*, 1789.

(4) (a) Segura, J. L.; Gómez, R.; Martín, N.; Luo, C.; Guldi, D. M. *Chem. Commun.* **2000**, 701. (b) Guldi, D. M.; Luo, C.; Swartz, A.; Gómez, R.; Segura, J. L.; Martín, N.; Brabec, C.; Sariciftci, N. S. *J. Org. Chem.* **2002**, *67*, 1141.

(5) (a) Nierengarten, J.-F.; Eckert, J.-F.; Nicoud, J.-F.; Ouali, L.; Krasnikov, V.; Hadziioannou, G. *Chem. Commun.* **1999**, 617. (b) Eckert, J.-F.; Nicoud, J.-F.; Nierengarten, J.-F.; Liu, S. G.; Armaroli, N.; Ouali, L.; Krasnikov, V.; Hadziioannou, G. *J. Am. Chem. Soc.* **2000**, *122*, 7467. (c) Armaroli, N.; Barigelleti, F.; Ceroni, P.; Eckert, J.-F.; Nicoud, J.-F.; Nierengarten, J.-F. *Chem. Commun.* **2000**, 599. (d) Yamashiro, T.; Aso, Y.; Otsubo, T.; Tang, H.; Harima, Y.; Yamashita, K. *Chem. Lett.* **1999**, 443. (e) Knorr, S.; Grupp, A.; Mehring, M.; Grube, G.; Effenberger, F. *J. Chem. Phys.* **1999**, *110*, 3502. (f) Peeters, E.; van Hal, P. A.; Knol, J.; Brabec, C. J.; Sariciftci, N. S.; Hummelen, J. C.; Janssen, R. A. J. *J. Phys. Chem. B* **2000**, *104*, 10174. (g) Martini, I.; Ma, B.; da Ros, T.; Helgeson, R.; Wudl, F.; Schwartz, B. *J. Chem. Phys. Lett.* **2000**, *327*, 253. (h) Obara, Y.; Takimiya, K.; Aso, Y.; Otsubo, T. *Tetrahedron Lett.* **2001,** *42*, 6877. (i) Liu, S.-G.; Martineau, C.; Raimundo, J.-M.; Echegoyen, L. *Chem. Commun.* **2001**, 913. (j) Gu, T.; Nierengarten, J.-F. *Tetrahedron Lett.* **2001**, *42*, 3175.

(6) (a) Segura, J. L.; Martín, N. *Tetrahedron Lett.* **1999**, *40*, 3239. (b) van Hal, P. A.; Knol, J.; Langeveld-Voss, B. M. W.; Meskers, S. C. J.; Hummelen, J. C.; Janssen, R. A. J. *J. Phys. Chem. A* **2000**, *104*, 5974. (c) Dhanabalan, A.; Knol, J.; Hummelen, J. C.; Jannsen, R. A. J. *Synth. Met.* **2001**, *119*, 519. (d) Martineau, C.; Blanchard, P.; Rondeau, D.; Delaunay, J.; Roncali, J. *Adv. Mater.* **2002**, *14*, 283.

(7) Prato, M.; Maggini, M. *Acc. Chem. Res.* **1998**, *31*, 519.

(8) (a) Martín, N.; Sánchez, L.; Illescas, B.; Pérez, I. *Chem. Rev.* **1998**, *98*, 2527. (b) Imahori, H.; Sakata, Y. *Adv. Mater.* **1997**, *9*, 537, (c) Imahori, H. Y. *J. Org. Chem.* **1999**, *64*, 2445.

(9) Gómez, R.; Segura, J. L.; Martín, N. *J. Org. Chem.* **2000**, *65*, 7501.

(10) Williams, R. M.; Zwier, J. M.; Verhoeven, J. W. *J. Am. Chem. Soc.* **1995**, *117*, 4093.

(11) (a) Suzuki, T.; Maruyama, Y.; Akasaba, T.; Ando, W.; Kobayashi, K.; Nagase, S. *J. Am. Chem. Soc.* **1994**, *116*, 1359. (b) Chlistouff, J.; Cliffel, D.; Bard, A. J. In *Handbook of Organic Conductive Molecules and Polymers*; Nalwa, N. S., Ed.; John Wiley & Sons: New York; 1997; Vol. 1, Chapter 7. (c) Echegoyen, L.; Echegoyen, L. E. *Acc. Chem. Res.* **1998**, *31*, 593.

(12) (a) Döttinger, S. E.; Hohloch, M.;. Segura, J. L.; Steinhuber, E.; Hanack, M.; Tompert, A.; Oelkrug, D. *Adv. Mater.* **1997**, *9*, 233. (b) Hohloch, M.; Segura, J. L.; Döttinger, S. E.; Hohnholz, D.; Steinhuber, E.; Spreitzer, H.; Hanack, M. *Synth. Met.* **1997**, *84*, 319.

(13) The oxidation wave of the remaining triads could not be observed under our experimental conditions or using toluene−acetonitrile as solvent mixture (4:1 v/v). However, the oxidation potential for 5b was identical to that measured for its related dyad (C_{60}−oligomer, ref 4b). From these data, we conclude that no significant differences were found between the oxidation potential values for dyads and triads.

(14) Shank, N. E.; Dorfman, L. M. *J. Chem. Phys* **1970**, *52*, 4441.

(15) For a review on fullerene excited states, see: Guldi, D. M.; Prato, M. *Acc. Chem. Res.* **2000**, *33*, 695.

(16) Guldi, D. M.; Maggini, M.; Scorrano, G.; Prato, M. *J. Am. Chem. Soc.* **1997**, *119*, 974.

(17) Zeng, Y.; Biczok, L.; Linschitz, H. *J. Phys. Chem.* **1992**, *96*, 5237. Guldi, D. M.; Asmus, K.-D. *J. Phys. Chem. A* **1997**, *101*, 1472. Guldi, D. M.; Maggini, M. *Gazz. Chim. Ital.* **1997**, *127*, 779.

(18) Marcus, R. A. *Angew. Chem., Int. Ed. Engl.* **1993**, *32*, 1111.

(19) Imahori, H.; Sakata, Y. *Eur. J. Org. Chem.* **1999**, 2445. Guldi, D. M. *Chem. Commun.* **2000**, 321. Fujitsuka, M.; Ito, O.; Yamashiro, T.; Aso, Y.; Otsubo, T. *J. Phys. Chem. A* **2000**, *104*, 4876.

(20) Thomas, M. D.; Hug, G. L. *Comput. Chem.* **1998**, *22*, 491.

(21) (a) Neta, P.; Huie, R. E. *J. Phys. Chem.* **1985**, *89*, 1783. (b) Armstrong, D. A.; Schuler, R. H. *J. Phys. Chem.* **1996**, *100*, 9892.

(22) Luo, C.; Fujitsuka, M.; Watanabe, A.; Ito, O.; Gan, L.; Huang, Y.; Huang, C.-H. *J. Chem. Soc., Faraday Trans.* **1998**, *94*, 527.

(23) Luo, C.; Fujitsuka, M.; Huang, C.-H.; Ito, O. *Phys. Chem. Chem. Phys.* **1999**, *1*, 2923.